Annals of Biomedical Engineering, Vol. 42, No. 5, May 2014 (© 2014) pp. 1085–1094
DOI: 10.1007/s10439-014-0981-0

Micro-Computed Tomography Based Computational Fluid Dynamics for the Determination of Shear Stresses in Scaffolds Within a Perfusion Bioreactor

EMILIE ZERMATTEN,[1] JOLANDA RITA VETSCH,[2] DAVIDE RUFFONI,[2,3] SANDRA HOFMANN,[2,4] RALPH MÜLLER,[2] and ALDO STEINFELD[1,5]

[1]Institute of Energy Technology, ETH Zurich, Zurich, Switzerland; [2]Institute for Biomechanics, ETH Zurich, Zurich, Switzerland; [3]Department of Aerospace and Mechanical Engineering, University of Liege, Liege, Belgium; [4]Orthopaedic Biomechanics Group, Eindhoven University of Technology, Eindhoven, The Netherlands; and [5]Solar Technology Laboratory, Paul Scherrer Institute, Villigen, Switzerland

(*Received 9 September 2013; accepted 20 January 2014; published online 4 February 2014*)

Associate Editor Scott I Simon oversaw the review of this article.

Abstract—Perfusion bioreactors are known to exert shear stresses on cultured cells, leading to cell differentiation and enhanced extracellular matrix deposition on scaffolds. The influence of the scaffold's porous microstructure is investigated for a polycaprolactone (PCL) scaffold with a regular microarchitecture and a silk fibroin (SF) scaffold with an irregular network of interconnected pores. Their complex 3D geometries are imaged by micro-computed tomography and used in direct pore-level simulations of the entire scaffold–bioreactor system to numerically solve the governing mass and momentum conservation equations for fluid flow through porous media. The velocity field and wall shear stress distribution are determined for both scaffolds. The PCL scaffold exhibited an asymmetric distribution with peak and plateau, while the SF scaffold exhibited a homogenous distribution and conditioned the flow more efficiently than the PCL scaffold. The methodology guides the design and optimization of the scaffold geometry.

Keywords—Scaffold, Bone tissue engineering, Perfusion bioreactor, Computational fluid dynamics, Direct pore-level simulations.

ABBREVIATIONS

CFD	Computational fluid dynamics
micro-CT	Micro-computed tomography
DPLS	Direct pore-level simulations
ECM	Extracellular matrix
PCL	Polycaprolactone
REV	Representative elementary volume
ROI	Region of interest
SF	Silk fibroin

Address correspondence to Aldo Steinfeld, Institute of Energy Technology, ETH Zurich, Zurich, Switzerland. Electronic mail: aldo.steinfeld@ethz.ch

NOMENCLATURE

$\boldsymbol{u}$	Velocity (m/s)
y	Height above the phase boundary (m)
μ	Dynamic viscosity (kg/m/s)
ρ	Density (kg/m^3)
τ_w	Wall shear stress (Pa)

INTRODUCTION

Regenerative approaches in clinical research are aimed at restoring functional, living tissues,[28] but are limited in their ability to up-scale *in vitro* grown constructs to clinically relevant sizes. To decipher the complexity of tissue engineering problems, the bottom-up approach[29] is applied to investigate a system spanning from small scales (e.g., cells) towards larger scales (e.g., cell aggregates, various tissue components) and finally to the full functional tissue. The main components constituting a tissue engineering culture are living cells, the scaffold, and the physicochemical culture environment. Scaffold properties play an important role in perfusion cultures. For instance, pore diameter, porosity, and pore interconnectivity have a

direct influence on the mechanical stimuli at the cellular level and on the cellular behavior.[4,44,46] Shear stresses increase with decreasing pore sizes[4] and decrease with increasing porosity.[46] To mimic the mechanical environment within healthy tissues and to reproduce the onset of diseases with *in vitro* models, it is important to know the mechanical stimuli a cell experiences at a given flow rate in a certain location within the scaffold. The present study investigates scaffolds in a controlled fluid dynamic environment using a perfusion bioreactor. Two scaffold types of different materials and geometries are considered.

Another important aspect examined in the present work is the application of mechanical stimulation through fluid flow within a perfusion bioreactor. Flow perfusion has been shown to increase cell number, improve the distribution of cells, increase the amount of deposited extracellular matrix (ECM) on the scaffold, and enhance the osteogenic phenotype.[2,5,8,12,36,37] The mechanical input was generated through the adaptation of the flow rate at the pump connected to the system. More important is the knowledge of the flow rate within the porous scaffold and the corresponding shear stresses exerted on cells attached to the scaffold surface. Evidently, the geometry of the bioreactor and of the scaffold has a great influence.

Simulations in bone tissue engineering were applied to predict the mechanical environment in bioreactor systems.[6,7,11,23] Several multiphysical models investigated tissue differentiation and growth in combination with mechanical environment simulations.[20,26] Computational fluid dynamics (CFD) simulations were especially suitable to predict shear stresses acting on cells as well as fluid velocities and pressures in scaffolds.[22] CFD simulations were also used in combination with micro-computed tomography (micro-CT) to define the geometry of the system.[7,23,33,45] However, because of computational limitations, only sub-volumes of the scaffolds were evaluated,[7,18] which introduced up to 30% variations in the calculated values because of the differences between these sub-volumes.[7,23] To avoid these inaccuracies, the minimal model size should be at least 10 times the average pore diameter.[23] Other simulations in the context of properties of porous materials recommended a minimal representative elementary volume (REV) size of at least 3.5 and up to 14 times the average pore diameter.[31,47] The size should be chosen even bigger for the determination of the pressure drop across a porous material.[47] In previous studies, micro-CT was used to obtain digital 3D representations of complex porous media and used in direct pore-level simulations (DPLS) for the determination of their effective transport properties.[9,13,14,47] Here, we applied the same computational methodology to characterize the transport phenomena in scaffolds within a perfusion bioreactor.

Specifically, the aim of this study is to determine the magnitude of wall shear stresses (τ_w) acting on cells seeded on the surface of the two scaffolds types within a perfusion bioreactor. The mechanical environment at the cellular level is simulated *via* micro-CT based DPLS of the entire scaffold–bioreactor construct. The main outputs are the flow velocity field and the τ_w distribution within the scaffold, which in turn determine the mechanical stimulation experienced by cells when subjected to perfusion flow. The knowledge of τ_w at each cell location on the scaffold surface guides the design and optimization of the scaffold geometry.

MATERIALS AND METHODS

Scaffolds and Perfusion Bioreactor System

Two scaffold types with different microarchitectures were considered. One scaffold type is made up of polycaprolactone (PCL) by free-form fabrication and has a rather regular microarchitecture.[3] The second scaffold type is made of silk fibroin (SF) by the salt leaching method and has a fairly irregular network of interconnected pores.[16,27,39,42] Both scaffolds have 8 mm-diameter, 3 mm-length cylindrical shape. Figure 1 shows the 3D rendering of the micro-CT scans of the two scaffold types: (a) PCL scaffold; and (b) SF scaffold. The scaffold pore diameter distributions are shown in Fig. 1c. The PCL scaffold was purchased from 3D Biotek.[3] According to the manufacturer, it has a nominal fiber diameter and fiber spacing of 300 μm. The fabrication of the SF scaffold was previously reported.[27] Briefly, cocoons from the silkworm *Bombyx mori* L. were boiled in 0.02 M Na_2CO_3 for 2 h, purified in ultrapure water, and dried. The dried silk was dissolved in 9 M LiBr solution (55 °C, 1 h), dialyzed, filtered, and frozen at −80 °C overnight. The frozen solution was freeze-dried and dissolved in 1,1,1,3,3,3-hexafluoro-2-propanol. Subsequently, 1 mL of the solution was mixed with 2.5 g NaCl granules (diameters 224–315 μm) and the organic solvent was then allowed to evaporate. β-sheet formation of SF was induced by immersion into 90% MeOH.[38] NaCl was extracted and the SF scaffolds were dried at room temperature.

Both scaffolds were introduced inside a perfusion bioreactor, as schematically depicted in Fig. 2. The perfusion system comprises (Fig. 2a): (1) a bioreactor housing; (2) a bag containing the culture medium; and (3) a peristaltic pump. The bioreactor housing (Fig. 2b) can be equipped with different inlays, allowing the testing of the two scaffolds configurations. Scaffolds are press-fit into the inlay to ensure a

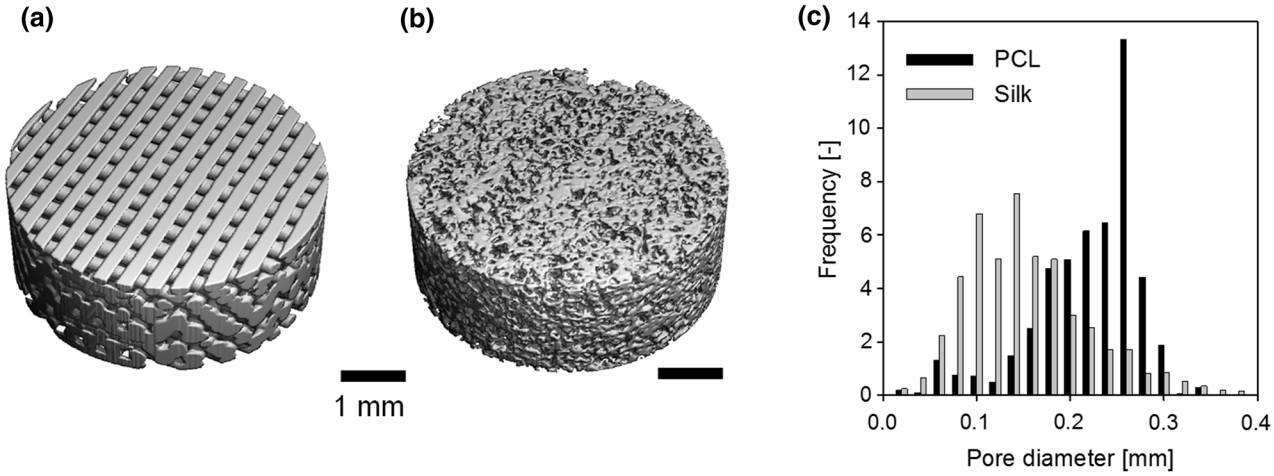

FIGURE 1. 3D rendering of micro-CT scans of the two scaffold types: (a) free-form fabricated polycaprolactone (PCL) scaffold and (b) silk fibroin (SF) scaffold. Both scaffolds have 8 mm-diameter, 3 mm-length cylindrical shape. (c) Scaffold pore diameter distributions.

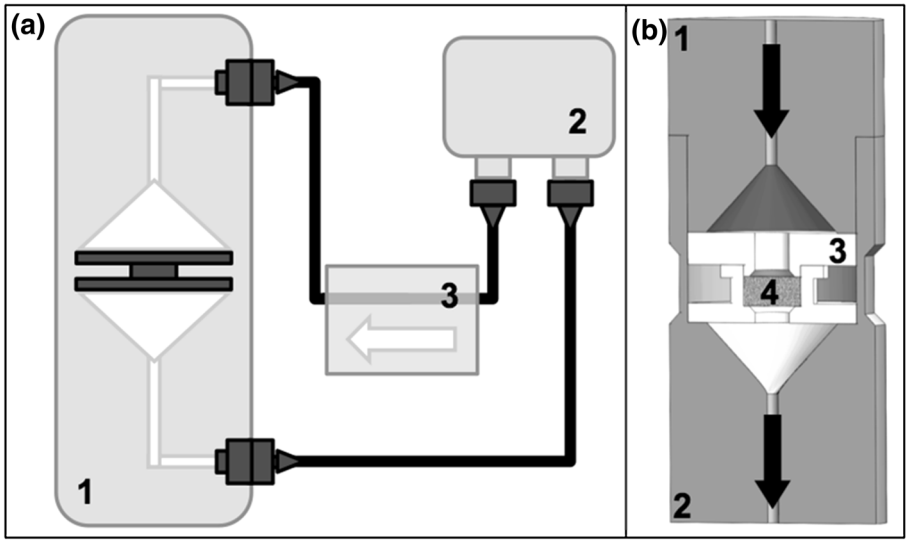

FIGURE 2. (a) Schematic of the bioreactor system, comprising: (1) the housing, (2) the media bag, and (3) the pump. (b) CAD drawing of the bioreactor geometry used for the DPLS: (1) bioreactor housing top, (2) bioreactor housing bottom, (3) inlay holding, and (4) scaffold. Flow direction is indicated by arrows.

confined setting exposed to the fluid flow. Because of the geometrical anisotropy of the (cylindrical) PCL scaffold, its orientation should be co-axial with the perfusion reactor (see Fig. 1a). The bioreactor system is compatible for μCT imaging: the housing can be separated from the rest of the perfusion system to perform μCT scans. This system design was successfully applied for perfusion studies using cell-seeded SF scaffolds.[43]

Micro-Computed Tomography (μCT)

The 3D microarchitecture of the two scaffolds was acquired non-destructively by μCT measurements. Both scaffolds were measured in dry state using a micro-CT (μCT40, Scanco Medical, Switzerland) operated at 45 kVp and 177 μA. An integration time of 200 ms and frame averaging of 4 were used, resulting in a total scanning time of approximately 2.4 h per sample. The reconstructed scans had a nominal isotropic resolution of 10 μm. After image reconstruction, a 3D Gaussian filter (SF: sigma = 0.8 and support = 1; PCL: sigma = 1.2 and support = 1) was applied to reduce the noise. The μCT data were then binarized using a global threshold corresponding to 4 and 4.5% of the maximum gray level for SF and PCL, respectively. Additionally, the sharp features that were present in the SF scaffold due to the drying process

were smoothed through the application of a Gaussian filter with sigma = 1 and support = 2 which reduced the local surface curvature. The scaffolds were then rescaled to a resolution of 20 μm and virtually cut to a cylindrical shape of 8 mm in diameter and 3 mm in length. This size corresponded to the size of the bioreactor inlay. Standard morphometric analysis was performed for both scaffolds to characterize pore diameter distribution.[40]

Mesh Generation and Sensitivity Analysis

The CFD domain is shown in Fig. 3 and consisted of the whole bioreactor housing (Fig. 2b) containing the scaffold. An in-house tetrahedron-based mesh generator[10] was used to create a computational grid directly from the digitalized geometry of the scaffold–bioreactor system. Initially, the mesh generator covered the entire domain with large tetrahedrons (initial edge length of 0.375 mm), which successively were gradually reduced in size according to a refinement process, followed by vertex rounding, cutting, and smoothing. Such procedure resulted in a highly refined mesh on small features (e.g., struts inside the scaffolds, Fig. 3c), and a coarser mesh far from the boundaries and for bigger features (e.g., bioreactor housing, Fig. 3b). A mesh sensitivity study was carried out to determine the influence of the number of refinements on the simulation outcomes. Specifically, the number of mesh refinements was fixed ($N = 2$) for the bioreactor whereas for the scaffolds it varied from 2 to 5. The convergence criterion applied for the mesh refinement was that the relative difference of the mean τ_w and $\boldsymbol{u}$ between two consecutive refinements was below 11%.

Computational Fluid Dynamics (CFD) Simulations

The commercial CFD code ANSYS,[1] based on the finite volume technique, was used to solve the 3D Navier–Stokes equations:

$$\frac{\partial \rho}{\partial t} + \nabla \cdot (\rho \boldsymbol{u}) = 0, \tag{1}$$

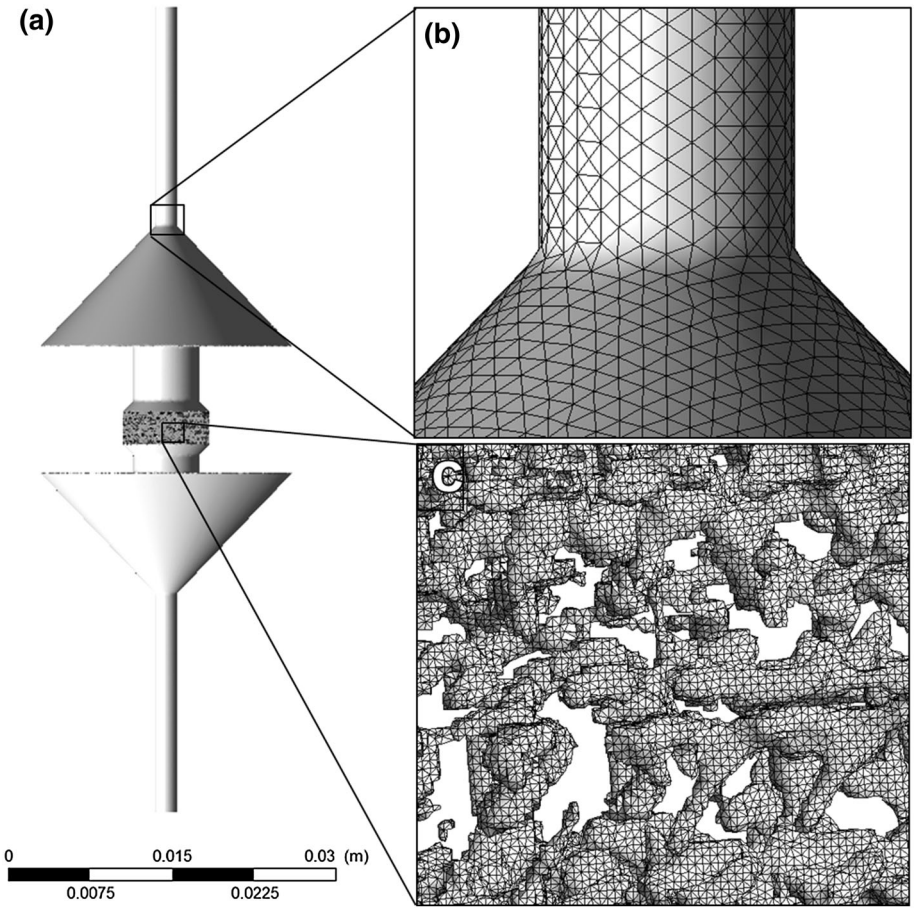

FIGURE 3. Computational domain: (a) bioreactor containing the scaffold. (b) The bioreactor is meshed with a coarse grid; smallest element size = 93.8 μm (before rounding, cutting, and smoothing). (c) The scaffold is meshed with a finer grid, smallest element size = 11.7 μm (before rounding, cutting, and smoothing).

TABLE 1. Results of the mesh sensitivity analysis: number of mesh refinements; minimum size of the resulting mesh elements; resulting number of elements; relative difference between two consecutive refinements in the mean τ_w and u.

	# Refinement	Min size (μm)	# Elements	%Δ τ_w	%Δ velocity
SF	2	93.8	5.11×10^5	77.0	29.0
	3	46.9	3.92×10^6	43.4	11.8
	4	23.4	2.33×10^7	10.9	2.2
	5	11.7	1.13×10^8	–	–
PCL	2	93.8	3.68×10^5	52.1	16.3
	3	46.9	2.46×10^6	17.1	3.7
	4	23.4	1.20×10^7	2.5	0.9
	5	11.7	5.58×10^7	–	–

$$\rho\left(\frac{\partial u}{\partial t} + \boldsymbol{u} \cdot \nabla \boldsymbol{u}\right) = -\nabla p + \mu \boldsymbol{u}, \tag{2}$$

where ρ is the density of the fluid, $\boldsymbol{u}$ the fluid velocity, and μ is the dynamic viscosity. The wall shear stress is defined as:

$$\tau_w = \mu \left.\frac{\partial u}{\partial y}\right|_{y=0}, \tag{3}$$

where y the height of the fluid above the phase boundary.

The computational domain is depicted in Fig. 3a. The boundary conditions were: inlet plug flow, a constant outlet pressure of 1 atm, and no-slip at the solid–fluid interface. Three different inlet flow rates were simulated, corresponding to the minimum (0.1 mL/min), average (0.2 mL/min), and maximum (0.3 mL/min) flow rates obtained with a standard laboratory pump. The culture medium was described as a homogeneous and incompressible Newtonian fluid, having density and dynamic viscosity of 997 kg/m^3 and 8.9×10^{-4} kg/m/s, respectively. The temperature of the culture medium was set to 37 °C, representing body temperature. Main simulation outcomes were the flow velocity and τ_w fields.

The frequency distributions of τ_w were averaged in five different regions of interest (ROI) along the scaffold length, each of thickness of 600 μm. The selected ROI did not include the scaffold–bioreactor interface of thickness of 100 and 140 μm for SF and PCL, respectively. These regions were excluded to avoid the influence of boundary artifacts.

RESULTS

Micro-Computed Tomography (μCT)

The μCT scans confirmed the regular structure of the PCL scaffold (Fig. 1a) and the irregular structure of the SF scaffold (Fig. 1b). As expected, the two scaffolds had different pore diameter distributions (Fig. 1c). For the PCL scaffold, the distribution was fairly asymmetric, peaked around 0.26 mm, with a mean of 0.22 ± 0.06 mm. For the SF scaffold, the distribution was bell-shaped, with a peak around 0.14 mm, and a mean of 0.16 ± 0.08 mm. The porosity of the PCL and SF scaffolds were 37.91 and 55.48%, respectively.

Mesh Sensitivity Analysis

Table 1 shows the results of the mesh sensitivity analysis. For each simulation, the number of refinements within the scaffold was increased, leading to smaller mesh elements. Mesh convergence was assessed by computing the relative difference between two consecutive refinements in mean τ_w and mean flow velocity. The mean τ_w was calculated by computing τ_w on each boundary element and averaging them. These two output parameters showed a quick convergence for the PCL scaffold with relative differences between refinements 5 and 4 less than 2.5% for mean τ_w and 1% for mean flow velocity. The simulations also converged well for the SF scaffold where the relative difference between the highest refined mesh (i.e., five refinements) and the one with four refinements was 11 and 2.2% for mean τ_w and mean flow velocity, respectively. Meshes with five refinements were used, yielding 59 and 115 million elements for the PCL and SF scaffolds, respectively. The minimum size of both meshes was 12 μm, corresponding to approximately half of the voxel size. The element diameter, defined as the longest length of an element in the mesh, was in average 22.86 and 21.55 μm for the PCL and SF scaffolds, respectively.

Computational Fluid Dynamics (CFD) Simulations

The frequency distributions of τ_w at an average flow rate of 0.2 ml/min for both scaffold geometries are shown in Fig. 4. The PCL scaffold exhibited a τ_w distribution shifted toward higher values from the entrance of the fluid flow (region 1, Fig. 4a) to the exit location (region 5, Fig. 4a). It became broader,

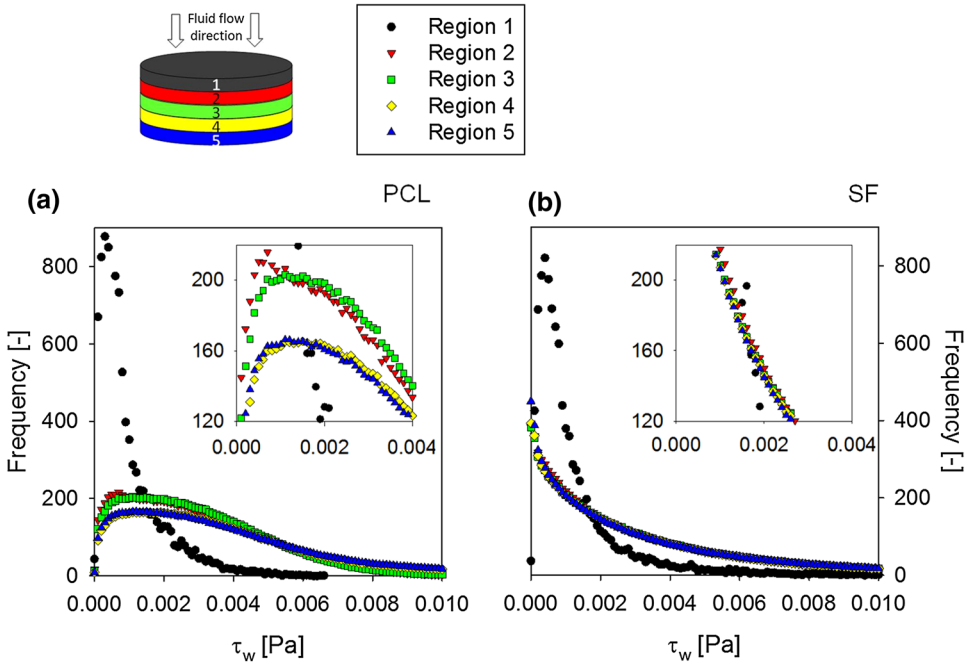

FIGURE 4. Frequency distribution of the wall shear stress in five different slices of the scaffold perpendicular to the flow (from entry to exit) for: (a) PCL scaffold and (b) SF scaffold. Inset: scheme of five regions of interest in the scaffold.

indicating a higher heterogeneity of τ_w in the regions 4 and 5. Moreover, the distributions relative to regions 2–5 showed a pronounced asymmetric peak with a plateau, being particularly flat in the regions 4 and 5. The SF scaffold exhibited identical τ_w distributions along its length of the scaffold, with exception of the entrance location (region 1, Fig. 4b), which showed a similar behavior as seen for the PCL scaffold. After a short travel distance through the scaffold, shear stresses were homogenous throughout the whole scaffold volume.

In practice, inlet flow rates can be adjusted through an external pump. The variation of the mean τ_w as a function of the inlet flow rates in the range 0.1–0.3 mL/min is shown in Fig. 5. For both scaffolds, a monotonically increasing linear correlation was obtained. The mean τ_w was minimal at the scaffold entrance (region 1) and increased towards downstream (regions 2–5). The slope of the lines in the five regions was dependent on the location along the scaffold. In accordance with the frequency distributions, mean τ_w values were similar between regions 2 and 3 and between regions 4 and 5 for the PCL scaffold, defining three regimes over the scaffold volume. In contrast, mean τ_w in regions 2, 3, 4, and 5 were almost identical for the SF scaffold, defining two regimes, one at the inlet and one throughout the rest of the scaffold. The 3D fluid flow streamlines across both scaffolds is shown in Fig. 6. The flow direction is from top to bottom. The scaffold is represented semi-transparent for a better visualization. The streamlines in the PCL scaffold showed a rather regular behavior, while those in the SF scaffold were random.

DISCUSSION

Using μCT-based DPLS, we have determined the τ_w distribution acting on the surfaces of two scaffold types commonly used in tissue engineering application.

Micro-Computed Tomography (μCT)

μCT was shown to be a suitable non-destructive technique to extract 3D morphological parameters of complex scaffold geometries for subsequent finite element simulations.[15] As polymeric scaffolds were scanned in their dry states in order to provide enough X-ray contrast, edged features were present especially in the SF scaffold where very fine structures close to the resolution limit were detected. In an *in vitro* culture, these scaffolds are hydrated by their surrounding aqueous environment, yielding smoother surface structures (data not shown). Consequently, a second smoothing procedure was applied to the SF scaffolds to reduce their local surface curvature. This reduction was more effective in regions were the surface curvature was high, and represented the swelling of the scaffold in the wet state by decreasing its porosity by about 12%. The eventual change in

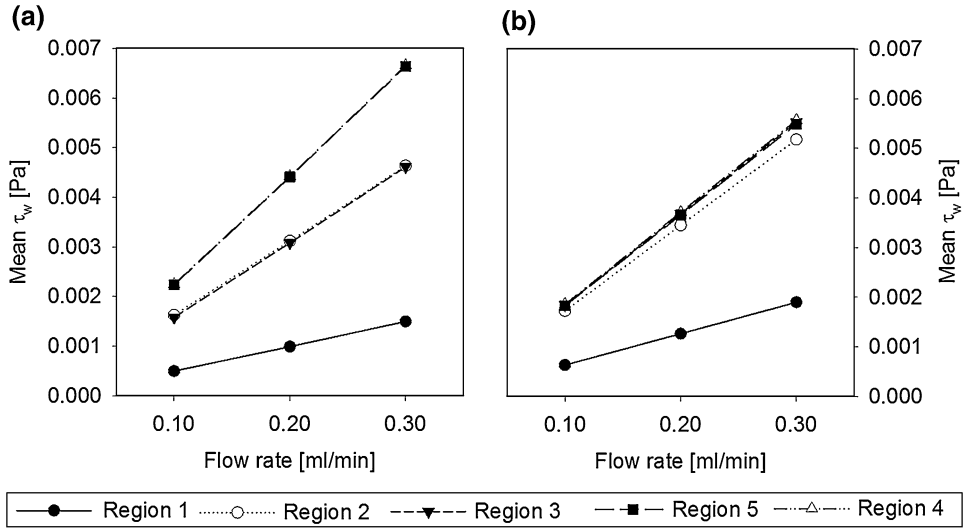

FIGURE 5. Mean wall shear stress as a function of the inlet flow rate for: (a) PCL scaffold and (b) SF scaffold. Each value represents the average of all τw values obtained in a slice of 600 μm in the five regions of interest.

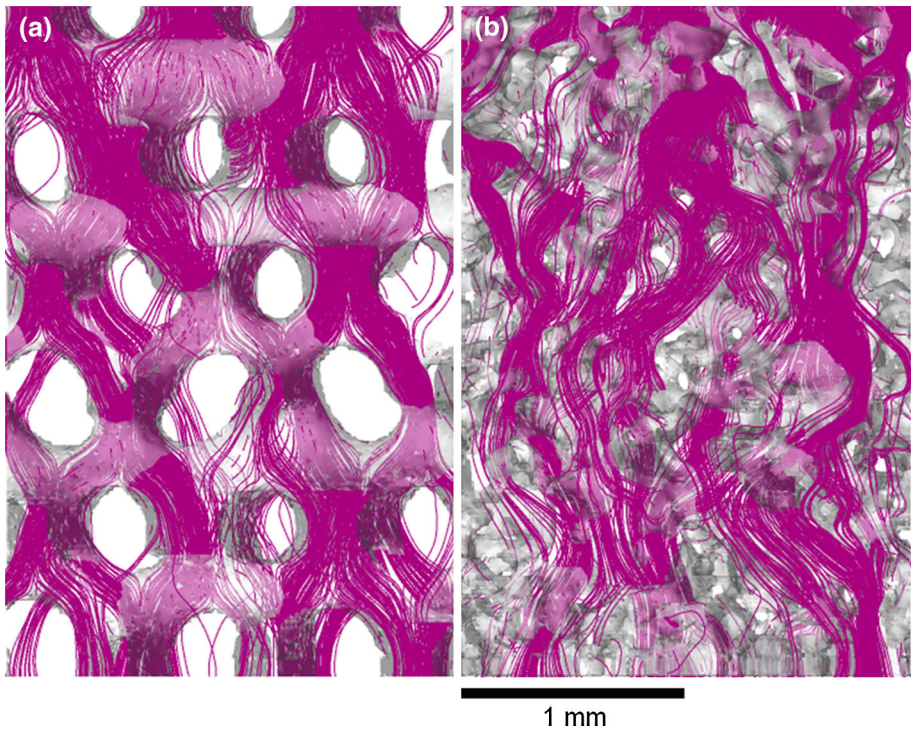

FIGURE 6. 3D fluid flow streamlines across: (a) PCL scaffold and (b) SF scaffold. Perfusion flow direction is from top to bottom.

porosity resulting from scaffold hydration[17] could not be determined because of the low contrast of μCT measurements of SF scaffolds in an aqueous environment. Estimations of surface structures and local curvature changes are based on visual inspections, histology, and SEMs.

Mesh Sensitivity Analysis

The mesh refinement study indicated the need of a highly refined mesh, especially for the SF scaffold. The simulations converged more rapidly with the PCL scaffold than with the SF scaffold. This is reflected in

Table 1, where less mesh cells were refined after the 4th refinement in the PCL scaffold, attributed to the larger and more regular pores in the PCL scaffold compared to those in the SF scaffold. At the highest mesh refinement (five refinements) the smallest mesh element length was 11.7 μm for both scaffolds, being already smaller than the final resolution of the μCT scan (20 μm). With relative differences smaller than 11% for τ_w and smaller than 2.2% for flow velocity, five refinements were considered sufficient for the present study. The resulting number of elements (59 million for the PCL scaffold and 115 million for the SF scaffold) is relatively high in terms of computational cost, but essential to enable the accurate geometrical representation of both scaffolds.

Computational Fluid Dynamics (CFD) Simulations

The scaffold–bioreactor system and boundary conditions mimic the cell experiments.[43] Field flow velocity and τ_w distributions were computed for the entire domain, taking into account the geometry of the bioreactor and of the scaffold. The simulated scaffold volume was bigger than the REV, defined as the smallest cubic volume to be considered as a continuum in a porous medium. Choosing a volume smaller than REV would affect the accuracy of the DPLS considerably.[41] Additionally, lateral boundary conditions would influence simulation results by up to 30% according to literature.[7,23] Here, the mean shear stress at the boundary of the reactor shows a decrease of 50% for PCL and 30% for SF. For the PCL scaffold, the diameter and length were 36 and 13 times larger than the mean pore diameter (0.22 ± 0.06 mm), respectively. For the SF scaffold, the diameter and length were 50 and 19 times larger than the mean pore diameter (0.16 ± 0.08 mm), respectively. The dimensions of both scaffolds were therefore larger than the suggested minimum REV, reported to be between 3.5 and 14 times the mean pore diameter.[23,47] The REV is even larger for the determination of pressure drop.[13,47] Furthermore, it has also been shown that the length of the sample parallel to the flow direction can be chosen 2–3 times shorter than the perpendicular length without affecting the precision of the results.[47]

Interestingly, both scaffolds showed a fairly similar τ_w behavior at the entrance region (region 1). On the other hand, the scaffold microarchitecture had a strong influence on the τ_w distribution in downstream regions. The smaller and irregular pores of the SF scaffold seemed to condition the flow more efficiently than the bigger pores of the PCL scaffold. Because of the channel-like geometry and the larger pore diameters of the PCL scaffold, the number of mesh cells experiencing a low τ_w increased and peaked. The peak was slightly shifted to the right as the inlet flow velocity increased, consistent with previous computational studies.[7,25,35] In contrast, no peaks or shoulders were observed in the SF scaffold. τ_w increased linearly with the inlet flow rate as expected for a laminar regime with Reynolds number maintained below 0.4, in accordance with other studies.[7,21,25]

An entrance flow rate of 0.2 mL/min (corresponding to a flow velocity of 0.066 mm/s) resulted in a mean τ_w of 3.08 mPa and of 3.68 mPa in the middle region (region 3) for PCL and SF scaffolds, respectively. The calculated mean τ_w were comparable to the values obtained in previous studies, as described in Table 2. Note that these previous studies simulated only the scaffold or part of it, and therefore suffered from uncertainties derived from using a computational domain smaller than REV and from omitting the bioreactor geometry. Shear stresses acting on cells seeded onto scaffolds have been shown to have an influence on cell viability, proliferation, and gene regulation.[33] Mean surface shear stresses of 5×10^{-5} Pa as calculated with the Lattice-Boltzmann method correlated to the highest cell viability at a flow rate of 0.01 mL/min.[33] However, because of a coarse resolution of 68 μm and because all lattice elements were of the same size, the L–B method lacked precision around small geometrical features and used excess elements around large ones. In contrast, our computational grid generator can be adapted efficiently to small and large geometrical features often encountered in complex bioreactor-scaffold configurations. Besides τ_w, other

TABLE 2. Comparison of obtained mean shear stress with other studies.

Study	Scaffold	Inlet velocity (mm/s)	Mean pore size (mm)	Porosity (%)	Mean τ_w (mPa)
Present study, PCL	Regular scaffold	0.066	0.22	37.91	3.08
Present study, SF	Irregular scaffold	0.066	0.16	55.48	3.68
Lesman *et al.*[21]	Regular scaffold	0.105	0.15	–	11
Van Ransbeeck *et al.*[41]	Irregular scaffold	0.034	0.275	70	1.1–1.95
Cioffi *et al.*[7]	Irregular scaffold	0.053	0.1	77	3.28–3.94
Maes *et al.*,[23] hydroxyapatite	Irregular scaffold	0.034	0.27	73	1.46
Maes *et al.*,[23] titanium	Irregular scaffold	0.034	0.28	77	1.95

mechanisms such as increased mass transport through the scaffold volume or flow streaming potentials can stimulate cells. Their effect may not be clearly differentiated from that of τ_w. Another limitation of the current work is that it did not take into account the volume of the seeded cells or the volume of the ECM produced by the cells. Our study solved the situation before cell seeding. After seeding, the cells fill up the spaces within the pores and, over time, they would surround themselves with ECM. This continuous obstruction of the pores would result in different τ_w acting on the cells due to decreased porosity and to shielding by ECM. To distinguish these time-dependent phenomena from each other, more advanced 3D monitoring is required.

The high computational cost is a drawback of this work. The domain of the scaffold should be selected large enough to enable the accurate determination the effective transport properties of the porous structure.[7,23,31,47] The bioreactor was also meshed to ensure an accurate representation of the flow field, but a coarser mesh was used outside the scaffold.

The PCL scaffold with a regular pore geometry gave rise to a peak τ_w. By controlling the scaffold architecture (porosity, pore size, *etc*.) in the manufacturing process, it may be possible to generate ranges of τ_w that promote a certain type of tissue formation.[19,24,30,34] In Lesman *et al*.,[21] an increase of the shear stress was observed when reducing the pore size of a regular scaffold. In the SF scaffold with irregular pore geometry, the flow chose preferable channels, as seen in Fig. 6b. Thus, to better understand the mechanical environment regulating cell behavior, a regular scaffold seemed more appropriate. The ultimate goal should be to predict the behavior of a cell-scaffold construct both *in vitro* and after implantation *in vivo*. Such prediction becomes even more essential when artificial matrices such as porous 3D scaffolds are applied as temporal supportive structures, as they considerably change the environment of the cells.[32] The methodology developed in this study enables to determine τ_w acting on the surface of scaffolds for tissue engineering. It further enables to examine and screen new scaffold designs for given shear stress levels, and thus avoid costly *in vitro* experiments.

ACKNOWLEDGMENTS

The authors gratefully acknowledge financial support from the European Union (BIODESIGN FP7-NMP-2010-LARGE-4). We thank H. Fries and A. Haselbacher for their support with the computational grid generation.

CONFLICT OF INTEREST

None.

REFERENCES

[1]Ansys. Ansys-CFX, 2009.
[2]Bancroft, G. N., V. I. Sikavitsas, J. van den Dolder, T. L. Sheffield, C. G. Ambrose, J. A. Jansen, and A. G. Mikos. Fluid flow increases mineralized matrix deposition in 3D perfusion culture of marrow stromal osteoblasts in a dose-dependent manner. *Proc. Natl. Acad. Sci.* 99(20):12600–12605, 2002.
[3]Biotek, D. 3D InsertTM PCL scaffold.
[4]Boschetti, F., M. T. Raimondi, F. Migliavacca, and G. Dubini. Prediction of the micro-fluid dynamic environment imposed to three-dimensional engineered cell systems in bioreactors. *J. Biomech.* 39(3):418–425, 2006.
[5]Botchwey, E., S. Pollack, E. Levine, and C. Laurencin. Bone tissue engineering in a rotating bioreactor using a microcarrier matrix system. *J. Biomed. Mater. Res.* 55(2):242–253, 2001.
[6]Byrne, D. P., D. Lacroix, J. A. Planell, D. J. Kelly, and P. J. Prendergast. Simulation of tissue differentiation in a scaffold as a function of porosity, Young's modulus and dissolution rate: application of mechanobiological models in tissue engineering. *Biomaterials* 28(36):5544–5554, 2007.
[7]Cioffi, M., F. Boschetti, M. T. Raimondi, and G. Dubini. Modeling evaluation of the fluid-dynamic microenvironment in tissue-engineered constructs: a micro-CT based model. *Biotechnol. Bioeng.* 93(3):500–510, 2006.
[8]David, V., A. Guignandon, A. Martin, L. Malaval, M.-H. Lafage-Proust, A. Rattner, V. Mann, B. Noble, D. B. Jones, and L. Vico. Ex vivo bone formation in bovine trabecular bone cultured in a dynamic 3D bioreactor is enhanced by compressive mechanical strain. *Tissue Eng. Part A* 14(1):117–126, 2008.
[9]Fredrich, J., A. DiGiovanni, and D. Noble. Predicting macroscopic transport properties using microscopic image data. *J. Geophys. Res. Solid Earth* (1978–2012). 111(B3), 2006.
[10]Friess, H., S. Haussener, A. Steinfeld, and J. Petrasch. Tetrahedral mesh generation based on space indicator functions. *Int. J. Numer. Methods Eng.* 93:1040–1056, 2012.
[11]Goldstein, A. S., T. M. Juarez, C. D. Helmke, M. C. Gustin, and A. G. Mikos. Effect of convection on osteoblastic cell growth and function in biodegradable polymer foam scaffolds. *Biomaterials* 22(11):1279–1288, 2001.
[12]Gomes, M. E., V. I. Sikavitsas, E. Behravesh, R. L. Reis, and A. G. Mikos. Effect of flow perfusion on the osteogenic differentiation of bone marrow stromal cells cultured on starch-based three-dimensional scaffolds. *J. Biomed. Mater. Res. Part A* 67(1):87–95, 2003.
[13]Haussener, S., P. Coray, W. Lipinski, P. Wyss, and A. Steinfeld. Tomography-based heat and mass transfer characterization of reticulate porous ceramics for high-temperature processing. *J. Heat Transfer* 132:023305, 2010.
[14]Haussener, S., and A. Steinfeld. Effective heat and mass transport properties of anisotropic porous ceria for solar thermochemical fuel generation. *Materials* 5(1):192–209, 2012.
[15]Ho, S. T., and D. W. Hutmacher. A comparison of micro CT with other techniques used in the characterization of scaffolds. *Biomaterials* 27(8):1362–1376, 2006.

[16]Hofmann, S., H. Hagenmüller, A. M. Koch, R. Müller, G. Vunjak-Novakovic, D. L. Kaplan, H. P. Merkle, and L. Meinel. Control of in vitro tissue-engineered bone-like structures using human mesenchymal stem cells and porous silk scaffolds. *Biomaterials* 28(6):1152–1162, 2007.
[17]Hofmann, S., K. S. Stok, T. Kohler, A. J. Meinel, and R. Müller. Effect of sterilization on structural and material properties of 3-D silk fibroin scaffolds. *Acta Biomater*. 10(1):308–317, 2014.
[18]Jungreuthmayer, C., S. W. Donahue, M. J. Jaasma, A. A. Al-Munajjed, J. Zanghellini, D. J. Kelly, and F. J. O'Brien. A comparative study of shear stresses in collagen-glycosaminoglycan and calcium phosphate scaffolds in bone tissue-engineering bioreactors. *Tissue Eng. Part A* 15(5):1141–1149, 2008.
[19]Kelly, D., and P. J. Prendergast. Mechano-regulation of stem cell differentiation and tissue regeneration in osteochondral defects. *J. Biomech*. 38(7):1413–1422, 2005.
[20]Lappa, M. Organic tissues in rotating bioreactors: fluid-mechanical aspects, dynamic growth models, and morphological evolution. *Biotechnol. Bioeng*. 84(5):518–532, 2003.
[21]Lesman, A., Y. Blinder, and S. Levenberg. Modeling of flow-induced shear stress applied on 3D cellular scaffolds: implications for vascular tissue engineering. *Biotechnol. Bioeng*. 105(3):645–654, 2010.
[22]Maes, F., T. Claessens, M. Moesen, H. Van Oosterwyck, P. Van Ransbeeck, and P. Verdonck. Computational models for wall shear stress estimation in scaffolds: a comparative study of two complete geometries. *J. Biomech*. 45(9):1586–1592, 2012.
[23]Maes, F., P. Van Ransbeeck, H. Van Oosterwyck, and P. Verdonck. Modeling fluid flow through irregular scaffolds for perfusion bioreactors. *Biotechnol. Bioeng*. 103(3):621–630, 2009.
[24]McGarry, J. G., J. Klein-Nulend, M. G. Mullender, and P. J. Prendergast. A comparison of strain and fluid shear stress in stimulating bone cell responses—a computational and experimental study. *FASEB J*. 19(3):482–484, 2005.
[25]Milan, J.-L., J. A. Planell, and D. Lacroix. Computational modelling of the mechanical environment of osteogenesis within a polylactic acid–calcium phosphate glass scaffold. *Biomaterials* 30(25):4219–4226, 2009.
[26]Milan, J.-L., J. A. Planell, and D. Lacroix. Simulation of bone tissue formation within a porous scaffold under dynamic compression. *Biomech. Model. Mechanobiol*. 9(5):583–596, 2010.
[27]Nazarov, R., H.-J. Jin, and D. L. Kaplan. Porous 3-D scaffolds from regenerated silk fibroin. *Biomacromolecules* 5(3):718–726, 2004.
[28]Nerem, R. Tissue engineering in the USA. *Med. Biol. Eng. Comput*. 30(4):CE8–CE12, 1992.
[29]Nichol, J. W., and A. Khademhosseini. Modular tissue engineering: engineering biological tissues from the bottom up. *Soft Matter* 5(7):1312–1319, 2009.
[30]Olivares, A. L., È. Marsal, J. A. Planell, and D. Lacroix. Finite element study of scaffold architecture design and culture conditions for tissue engineering. *Biomaterials* 30(30):6142–6149, 2009.
[31]Petrasch, J., P. Wyss, and A. Steinfeld. Tomography-based Monte Carlo determination of radiative properties of reticulate porous ceramics. *J. Quant. Spectrosc. Radiat. Transfer* 105(2):180–197, 2007.
[32]Place, E. S., N. D. Evans, and M. M. Stevens. Complexity in biomaterials for tissue engineering. *Nat. Mater*. 8(6):457–470, 2009.
[33]Porter, B., R. Zauel, H. Stockman, R. Guldberg, and D. Fyhrie. 3-D computational modeling of media flow through scaffolds in a perfusion bioreactor. *J. Biomech*. 38(3):543–549, 2005.
[34]Sandino, C., and D. Lacroix. A dynamical study of the mechanical stimuli and tissue differentiation within a CaP scaffold based on micro-CT finite element models. *Biomech. Model. Mechanobiol*. 10(4):565–576, 2011.
[35]Sandino, C., J. Planell, and D. Lacroix. A finite element study of mechanical stimuli in scaffolds for bone tissue engineering. *J. Biomech*. 41(5):1005–1014, 2008.
[36]Sikavitsas, V. I., G. N. Bancroft, H. L. Holtorf, J. A. Jansen, and A. G. Mikos. Mineralized matrix deposition by marrow stromal osteoblasts in 3D perfusion culture increases with increasing fluid shear forces. *Proc. Natl. Acad. Sci*. 100(25):14683–14688, 2003.
[37]Sikavitsas, V. I., G. N. Bancroft, J. J. Lemoine, M. A. Liebschner, M. Dauner, and A. G. Mikos. Flow perfusion enhances the calcified matrix deposition of marrow stromal cells in biodegradable nonwoven fiber mesh scaffolds. *Ann. Biomed. Eng*. 33(1):63–70, 2005.
[38]Tsukada, M., Y. Gotoh, M. Nagura, N. Minoura, N. Kasai, and G. Freddi. Structural-changes of silk fibroin membranes induced by immersion in methanol aqueous-solutions. *J. Polym. Sci. B* 32(5):961–968, 1994.
[39]Uebersax, L., H. Hagenmüller, S. Hofmann, E. Gruenblatt, R. Müller, G. Vunjaknovakovic, D. L. Kaplan, H. Merkle, and L. Meinel. Effect of scaffold design on bone morphology in vitro. *Tissue Eng*. 12(12):3417–3429, 2006.
[40]van Lenthe, G. H., H. Hagenmüller, M. Bohner, S. J. Hollister, L. Meinel, and R. Müller. Nondestructive micro-computed tomography for biological imaging and quantification of scaffold–bone interaction in vivo. *Biomaterials* 28(15):2479–2490, 2007.
[41]Van Ransbeeck, P., F. Maes, S. Impens, H. Van Oosterwyck, and P. Verdonck. Numerical modeling of perfusion flow in irregular scaffolds. In: 4th European Conference of the International Federation for Medical and Biological Engineering, 2009, pp. 2677–2680.
[42]Vepari, C., and D. L. Kaplan. Silk as a biomaterial. *Prog. Polym. Sci*. 32(8):991–1007, 2007.
[43]Vetsch, J. R., S. Hofmann, and R. Müller. Increased flow velocity positively influences osteogenic differentiation of human stem cells in a perfusion bioreactor. In: 3rd Termis World Congress, 2012.
[44]Vetsch, J. R., R. Müller, and S. Hofmann. The evolution of simulation techniques for dynamic bone tissue engineering in bioreactors. *J. Tissue Eng. Regen. Med*., 2013. doi: 10.1002/term.1733.
[45]Voronov, R., S. VanGordon, V. I. Sikavitsas, and D. V. Papavassiliou. Computational modeling of flow-induced shear stresses within 3D salt-leached porous scaffolds imaged via micro-CT. *J. Biomech*. 43(7):1279–1286, 2010.
[46]Yao, Y., Y. Yu, J. Guo, Y. Qian, and J. Wang. Prediction of shear stress distribution throughout 3D bone scaffold in perfusion environment. In: 2010 International Conference on Image Analysis and Signal Processing (IASP), 2010, pp. 51–54.
[47]Zermatten, E., S. Haussener, M. Schneebeli, and A. Steinfeld. Tomography-based determination of permeability and Dupuit-Forchheimer coefficient of characteristic snow samples. *J. Glaciol*. 57(205):811–816, 2011.